Mechanism and Machine Theory 45 (2010) 200–211

Contents lists available at ScienceDirect

Mechanism and Machine Theory

journal homepage: www.elsevier.com/locate/mechmt

Optimum design of spherical parallel manipulators for a prescribed workspace

Shaoping Bai *

Department of Mechanical Engineering, Aalborg University, Denmark

ARTICLE INFO

Article history:
Received 23 July 2007
Received in revised form 18 November 2008
Accepted 28 June 2009
Available online 21 October 2009

Keywords:
Spherical parallel manipulator
Design space
Numerical optimization
Workspace analysis
Dexterity

ABSTRACT

The optimum design of spherical parallel manipulators (SPM) is studied for a prescribed workspace. A numerical method is developed to find optimal design parameters including link dimensions and architecture parameters for a maximum dexterity. In the method, the objective function is formulated in such a way that the optimal problem is converted to a nonlinear least squares problem, which can be readily solved. Moreover, the problem of design space is addressed. A system of inequalities in terms of link dimensions is derived to describe the design space for feasible SPMs. Examples are included to illustrate the application of the method.

1. Introduction

A spherical parallel manipulator (SPM) is in general made up of two pyramid-shape platforms, namely, the base platform and the mobile platform that are connected by three equally spaced legs, each consisting of revolute joints only. The axes of all joints intersect at a common point, which is called the center of rotation. The motion of the mobile platform is confined on the surface of a sphere centered at the rotation center, thereby a spherical parallel manipulator provides three degrees of freedom of pure rotations. Most applications of SPMs can be found in orienting devices as Fig. 1a, such as camera orienting and medical instrument alignment [1–3]. They can also be used to develop spherically actuated manipulators, as demonstrated in Fig. 1b. While most SPMs studied are of three dofs, SPMs with two dofs were also reported [4].

In designing spherical parallel manipulators, a common concern is the workspace [5–8]. In general, the workspace of an SPM is rather small due to the characteristic of its closed kinematic chain, a design with large workspace is desirable. It is already shown in [9] that an SPM has the maximum workspace if the two links of each leg have identical dimensions of 90°. On the other hand, a high kinematic performance within the workspace is required. A commonly used index to quantify the kinematic performance is dexterity [5]. While the workspace volume and dexterity cannot reach maximum simultaneously [10], optimum design can be carried out with preference on one of them. In this work, the optimum design is confined to find optimal design parameters in terms of dexterity over a prescribed workspace.

Some optimum kinematic designs for SPMs have been reported in the literature. Asada and Granito followed a graphic approach in which they examined graphically the condition number with different sets of geometrical parameters [11]. Gosselin and Angeles made use of the bisection searching method for minimizing the conditioning index [9]. A genetic algorithm was adopted by Li and Payandeh in finding the optimal design of a medical SPM [2]. Liu et al. investigated the SPM optimization considering both dexterity and stiffness [7]. Other relevant works of optimum design can be found in [12,13].

* Tel.: +45 9940 9291; fax: +45 9815 1675.
E-mail addresses: shb@me.aau.dk, baishaoping@yahoo.com

0094-114X/$ - see front matter © 2009 Elsevier Ltd. All rights reserved.
doi:10.1016/j.mechmachtheory.2009.06.007

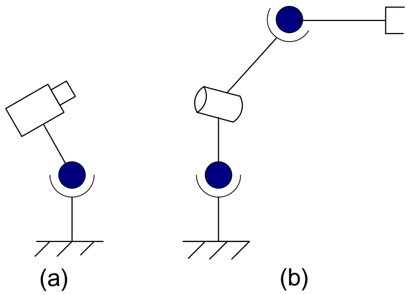

Fig. 1. Applications of SPMs: (a) an orienting device and (b) a spherically actuated manipulator.

In the optimum design, three issues have to be considered. The first one is the criteria of optimization. In the kinematic design, a commonly used criterion is the dexterity, which, in this work, refers to the capacity of an SPM to provide a large range of orientation to its end-effector. Dexterity describes generally an SPM's motion accuracy, controllability (singularity), and manipulability. There are different definitions to characterize the dexterity [11,14,15]. The earliest definition of dexterity is introduced by Salisbury and Craig [14], in which the dexterity is evaluated by the condition number of the Jacobian matrix. Other definitions include the Generalized Velocity Ratios, in short GVR, by Asada and Granito [11], and the Global Conditioning Index, GCI, by Gosselin and Angeles [15]. The GCI takes the average value of the reciprocal of the condition number over the workspace volume. More dexterity definitions can be found in [16,17]. In addition to the dexterity, other criteria including stiffness and forces at the actuators are also considered in some studies. In this work, the author adopts the GCI convention, with the aim to evaluate dexterity over a given workspace.

The second issue is concerned with the selection of a proper optimization method, which can be either numerical and graphic one [11,12]. A graphic method displays directly the variations of performance indices, from which optimum solutions can be obtained. The shortage is that only a very limited number of parametric selections can be investigated, which may lead to sub-optimal results, as revealed in the examples of this paper. Moreover, graphic methods are less effective if the design space contains more than three variables. On the other hand, a numerical method is capable to handle with large design space in the SPM optimization. The problem with numerical methods is that they are normally very time-consuming, partly due to the calculation of the performance index and partly to the definition of objective function, which are problems addressed in the paper.

The last issue is on the determination of design space. Design space describes the bounds for all design variables. The design space enables designers to gain an insight into the problem with feasible solutions. To some extent, the importance of the design space is often overlooked in optimum designs, only a few studies being concerned with the design space [7,18,19]. As a matter of fact, a well defined design space can contribute to the finding of an optimal solution by confining the search or calculation with values that lead to a feasible mechanism. The constraints on the possible values of design parameters are especially important to numerical methods, for which the output depends highly on the initial points within the design space. For this reason, the design space can provide a guidance to the selection of initial values in numerical optimizations.

In this work, the optimum design of spherical parallel manipulators with a prescribed workspace is studied with an aim to determine the design space and, furthermore, to find optimal design parameters in terms of dexterity. A system of inequalities is derived to describe the design space of possible design parameters such as link dimensions and other geometrical parameters. A numerical optimization is finally formulated for SPMs as a nonlinear least squares problem. The study is conducted with respect to a spherical parallel manipulator with coaxial input shafts.

The paper is organized as follows: First, a conceptual design of an SPM with coaxial input shafts is presented in Section 2. The forward and inverse kinematics of SPMs are reviewed in Section 3. The design space problem is solved in Section 4. An optimum design method is developed in Section 5. Design examples are included in Section 6. The work is concluded in Section 7.

2. An SPM with coaxial input shafts

The spherical parallel manipulator in the work is a novel robotic wrist capable of unlimited rolling motion. As shown in Fig. 2a, the SPM consists of three curved links connected to a mobile platform as an end-effector. The three links are driven by three actuators moving independently on a circular guide. The manipulator has three kinematic chains made up of two revolute and one spherical joints,[1] it hence being classified as a 3-RRS wrist. Degrees of freedom of the SPM are determined through Grubler formula as

$$m = 6(n_l - 1) - 5n_r - 3n_s = 6 \times (8 - 1) - 5 \times 6 - 3 \times 3 = 3 \tag{1}$$

where n_l is the number of total links and n_r and n_s are numbers of revolute and spherical joints, respectively.

[1] The sliders that move one the circular guide are also called *circular prismatic* joints, as addressed in [20].

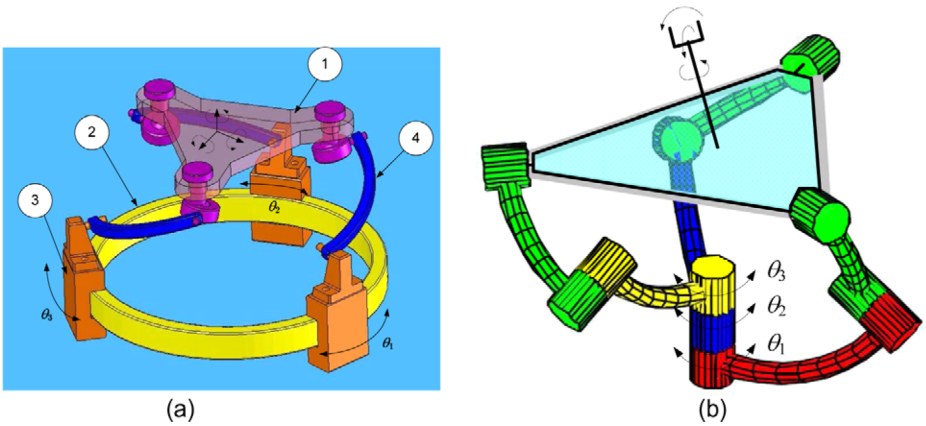

Fig. 2. An SPM capable of unlimited rolling: (a) conceptual design with (1) end-effector, (2) circular guide, (3) actuating unit and (4) curved link; and (b) its equivalent SPM model.

The described design is kinematically equivalent to an SPM with coaxial input shafts as shown in Fig. 2b, which was first reported in [11]. Such a coaxial architecture enables the SPM have an unlimited rolling, in addition to limited pitch and yaw rotations. Compared with Fig. 2b, the embodiment of Fig. 2a improves the design in several aspects. First, the use of circular guide eliminates the three curved links connected to input shafts and keeps only the three links supporting the mobile platform. As a matter of fact, circular tracks that support sliders can be found in some robotic applications [21,22]. By introducing the circular guide, the SPM can be designed using a modular approach, now that all three legs are identical. Moreover, the stiffness of each leg is improved due to the presence of the circular guide. Furthermore, the upper curved links and the mobile platform are connected by spherical joints, rather than revolute ones, which prevent the occurrence of overconstraint of physical revolute joints. This can be seen from Eq. (1), where no repeated constraint is found. From a mechanism viewpoint, the SPM introduced has the same kinematic features as a ball joint and is referred as an *active ball joint*.

3. Kinematics of SPM

A general spherical parallel manipulator is shown in Fig. 3a. The SPM consists only of revolute joints, whose axes are denoted by unit vectors $\mathbf{u}_i$, $\mathbf{v}_i$, and $\mathbf{w}_i$. The three links that are connected to the base platform have identical dimensions of α_1, while the three links that connect to the mobile platform have identical dimensions of α_2. Moreover, β and γ define the geometry of two regular pyramids of the base and mobile platforms. The active ball joint is a special case of SPMs for which $\gamma = 0$.

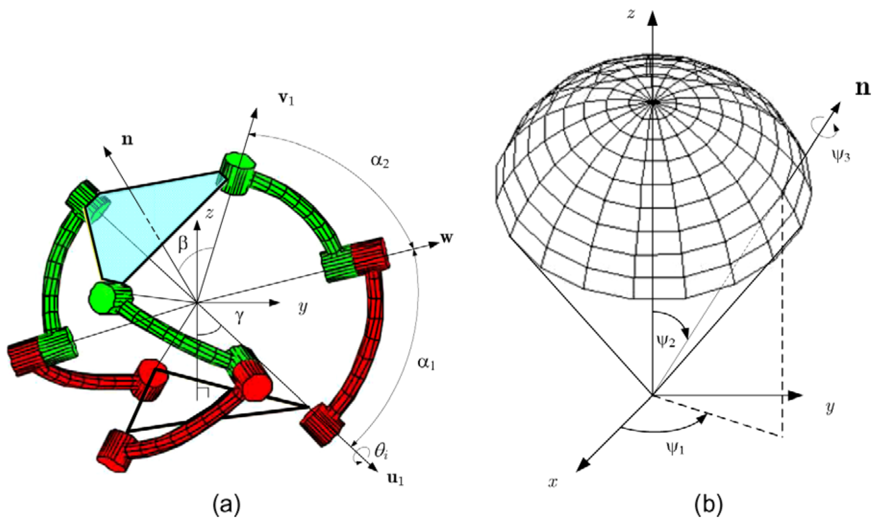

Fig. 3. Kinematic model of a spherical parallel manipulator: (a) symbol convention and (b) prescribed workspace.

A coordinate system is selected for the SPM, with the origin located at the rotation center. The z axis is normal to the bottom surface of the base pyramid and points upwards, while the y axis is located in the plane made by the z axis and $\mathbf{u}_1$.

Refer to Fig. 3b, the orientation of SPM is described by an array of angles $\boldsymbol{\psi} = [\psi_1, \psi_2, \psi_3]^T$, for which the rotation matrix is defined by two sequential rotations

$$\mathbf{Q} = rot(\mathbf{e}_2, \psi_2) rot(\mathbf{e}_3, \psi_3) \tag{2}$$

where $\mathbf{e}_2 = [-\sin\psi_1, \cos\psi_1, 0]^T$, $\mathbf{e}_3 = [0, 0, 1]^T$ and $rot(\mathbf{e}_i, \psi_i)$ is a rotation matrix following the angle-axis representation [23].

Under the selected coordinate system, unit vector $\mathbf{u}_i$ is derived as:

$$\mathbf{u}_i = [-\sin\eta_i \sin\gamma, \cos\eta_i \sin\gamma, -\cos\gamma]^T \tag{3}$$

where $\eta_i = 2(i-1)\pi/3$.

Unit vector $\mathbf{w}_i$, $i = 1, 2, 3$ of the axis of the intermediate revolute joint of the ith leg is obtained in terms of the input joint angle θ_i, $i = 1, 2, 3$ as:

$$\mathbf{w}_i = \mathbf{R}_i \mathbf{z}_y \tag{4}$$

where $\mathbf{z}_y = [0, 1, 0]^T$ and $\mathbf{R}_i = rot(\mathbf{u}_i, \theta_i)$. Expanding the right side of Eq. (4) yields

$$\mathbf{w}_i = \begin{bmatrix} -s\eta_i s\gamma c\alpha_1 + (c\eta_i s\theta_i - s\eta_i c\gamma c\theta_i) s\alpha_1 \\ c\eta_i s\gamma c\alpha_1 + (s\eta_i s\theta_i + c\eta_i c\gamma c\theta_i) s\alpha_1 \\ -c\gamma c\alpha_1 + s\gamma c\theta_i s\alpha_1 \end{bmatrix} \tag{5}$$

where s stands for *sine*, and c for *cosine*.

Unit vector $\mathbf{v}_i$, parallel to the axis of the top revolute joint of the ith leg, is a function of the orientation of the mobile platform. Let this orientation be described by the rotation matrix $\mathbf{Q}$, then

$$\mathbf{v}_i = \mathbf{Q}\mathbf{v}_i^* \tag{6}$$

where $\mathbf{v}_i^*$ is the unit vector for the axis of the top revolute joint of the ith leg when the mobile platform is in its reference orientation, which is given as

$$\mathbf{v}_i^* = [-\sin\eta_i \sin\beta, \cos\eta_i \sin\beta, \cos\beta]^T \tag{7}$$

For the closed chain of the spherical parallel manipulator, the following equation holds:

$$\mathbf{w}_i \cdot \mathbf{v}_i = \cos\alpha_2, \quad i = 1, 2, 3 \tag{8}$$

The Jacobian matrix of SPMs can be obtained through differentiating Eq. (8), which gives

$$\dot{\mathbf{w}}_i \cdot \mathbf{v}_i + \mathbf{w}_i \cdot \dot{\mathbf{v}}_i = 0 \tag{9a}$$

Note that

$$\dot{\mathbf{v}}_i = \boldsymbol{\omega} \times \mathbf{v}_i \tag{9b}$$

$$\dot{\mathbf{w}}_i = \dot{\theta}_i \mathbf{u}_i \times \mathbf{w}_i \tag{9c}$$

where $\boldsymbol{\omega}$ is the angular velocity of the end-effector. Eq. (9a) is finally written in a form of

$$\mathbf{J}\boldsymbol{\omega} = \dot{\boldsymbol{\theta}} \tag{9d}$$

where $\dot{\boldsymbol{\theta}} = [\dot{\theta}_1, \dot{\theta}_2, \dot{\theta}_3]^T$, and $\mathbf{J} = [\mathbf{j}_1, \mathbf{j}_2, \mathbf{j}_3]^T$ with $\mathbf{j}_i = \frac{\mathbf{w}_i \times \mathbf{v}_i}{(\mathbf{u}_i \times \mathbf{w}_i) \cdot \mathbf{v}_i}$.

4. Determination of design space

Substituting Eqs. (5) and (6) into Eq. (8) and further substituting the tan-half identifies, namely,

$$\cos\theta_i = \frac{1 - t_i^2}{1 + t_i^2}, \quad \sin\theta_i = \frac{2t_i}{1 + t_i^2}, \quad t_i = \tan(\theta_i/2) \tag{10}$$

into the new equation produces

$$A_i t_i^2 + 2B_i t_i + C_i = 0, \quad i = 1, 2, 3 \tag{11}$$

where A_i, B_i and C_i are functions of the kinematic parameters and of the orientation of the mobile platform. The presence of real solutions of t_i implies that the discriminant of Eq. (11) has to be non-negative, i.e.

$$B_i^2 - A_i C_i \geqslant 0, \quad i = 1, 2, 3 \tag{12}$$

from which the design space is to be determined. For simplicity, we first deal with leg 1 only, for which $\eta_i = \eta_1 = 0$.

Let $\mathbf{v}_i = [x_i, y_i, z_i]^T$. The coefficient functions A, B and C of Eq. (11) become

$$A_i = y_i(\mathrm{s}\gamma\mathrm{c}\alpha_1 - \mathrm{c}\gamma\mathrm{s}\alpha_1) - z_i(\mathrm{c}\gamma\mathrm{c}\alpha_1 + \mathrm{s}\gamma\mathrm{s}\alpha_1) - \mathrm{c}\alpha_2 \tag{13a}$$

$$B_i = x_i\mathrm{s}\alpha_1 \tag{13b}$$

$$C_i = y_i(\mathrm{s}\gamma\mathrm{c}\alpha_1 + \mathrm{c}\gamma\mathrm{s}\alpha_1) - z_i(\mathrm{c}\gamma\mathrm{c}\alpha_1 - \mathrm{s}\gamma\mathrm{s}\alpha_1) - \mathrm{c}\alpha_2 \tag{13c}$$

where $i = 1$. By substituting Eqs. (13a)–(13c) into Eq. (12) and simplifying, we have

$$[x_i^2 + (y_i\mathrm{c}\gamma + z_i\mathrm{s}\gamma)^2]\mathrm{s}^2\alpha_1 - [(y_i\mathrm{s}\gamma - z_i\mathrm{c}\gamma)\mathrm{c}\alpha_1 - \mathrm{c}\alpha_2]^2 \geqslant 0, \quad i = 1 \tag{14a}$$

A tedious manipulation on the above equation, making use of $x_i^2 + y_i^2 + z_i^2 = 1$ and trigonometric identities, finally yields

$$-(y_i\mathrm{s}\gamma - z_i\mathrm{c}\gamma - \mathrm{c}\alpha_1\mathrm{c}\alpha_2)^2 + \mathrm{s}^2\alpha_1\mathrm{s}^2\alpha_2 \geqslant 0 \tag{14b}$$

which is further written as

$$(y_i\mathrm{s}\gamma - z_i\mathrm{c}\gamma - d_1)(y_i\mathrm{s}\gamma - z_i\mathrm{c}\gamma - d_2) \leqslant 0, \quad i = 1 \tag{14c}$$

or

$$\prod_{j=1}^{2}(y_i\mathrm{s}\gamma - z_i\mathrm{c}\gamma - d_j) \leqslant 0, \quad i = 1 \tag{14d}$$

where $d_j \equiv \cos(\alpha_1 + (-1)^j\alpha_2),\ j = 1, 2$.

Inequality (14d) for leg 1 can be generalized for the other two legs by coordinate transformation, which yields

$$\prod_{j=1}^{2}(-x_i\mathrm{s}\eta_i\mathrm{s}\gamma + y_i\mathrm{c}\eta_i\mathrm{s}\gamma - z_i\mathrm{c}\gamma - d_j) \leqslant 0, \quad i = 1, 2, 3 \tag{15}$$

that is

$$\prod_{j=1}^{2}(\mathbf{n}_i^T\mathbf{v}_i + d_j) \leqslant 0, \quad i = 1, 2, 3 \tag{16}$$

where $\mathbf{n}_i = [\mathrm{s}\eta_i\mathrm{s}\gamma, -\mathrm{c}\eta_i\mathrm{s}\gamma, \mathrm{c}\gamma]^T$.

Let $f_i = \mathbf{n}_i^T\mathbf{v}_i$ which is bounded by $\max(f_i)$ and $\min(f_i)$. For any given β and γ, f_i becomes a function of x_i, y_i and z_i, which are functions of SPM orientation. Now that $x_i^2 + y_i^2 + z_i^2 = 1$, the determination of the maximum and minimum of f_i is actually a constrained optimization problem, which can be solved numerically.

With $\max(f_i)$ and $\min(f_i)$, the inequality of (16) leads to two systems of inequalities, which are

$$-\cos(\alpha_1 + \alpha_2) \leqslant \min(f_i) \tag{17a}$$

$$-\cos(\alpha_1 - \alpha_2) \geqslant \max(f_i) \tag{17b}$$

and

$$-\cos(\alpha_1 - \alpha_2) \leqslant \min(f_i) \tag{17c}$$

$$-\cos(\alpha_1 + \alpha_2) \geqslant \max(f_i) \tag{17d}$$

By graphically checking on the systems, it can be found that the inequalities of (17a) and (17b) yield four unbounded regions for solutions, where unlikely the feasible link dimensions are found. The feasible solutions can only be found by the inequalities of (17c) and (17d), which can be rewritten as

$$-\cos(\alpha_1 - \alpha_2) \leqslant f_{min} \tag{18a}$$

$$-\cos(\alpha_1 + \alpha_2) \geqslant f_{max} \tag{18b}$$

where $f_{min} = \min\{f_i\}_1^3$ and $f_{max} = \max\{f_i\}_1^3$. By assuming $\alpha_1 \in (0, 180^\circ]$ and $\alpha_2 \in (0, 180^\circ]$, the inequalities (18a) and (18b) lead to

$$|\alpha_1 - \alpha_2| \leqslant \cos^{-1}(-f_{min}) \tag{19a}$$

$$|\alpha_1 + \alpha_2 - 180^\circ| \leqslant \cos^{-1}(f_{max}) \tag{19b}$$

The left sides of the inequalities (19a) and (19b) are of link dimensions, while the right sides are functions of geometrical parameters γ and β. When plotted in the $\alpha_1 - \alpha_2$ plane, the system of inequalities yields a rectangular region. Any point in the rectangle stands for a pair of feasible dimensions for the prescribed workspace. In light of this, the two inequalities are referred as *design space inequalities*.

5. Optimization of design parameters

The design space enables us select the possible design parameters for a prescribed workspace. To find the optimal parameters within the design space for a better kinematic performance, a certain means of optimization has to be employed. The optimization in this work is conducted numerically on a nonlinear square problem formulated by modifying the criteria of evaluation, as described presently.

5.1. Dexterity evaluation

Prior to optimizations, a criterion has to be selected first for evaluation of the dexterity of SPMs. A commonly used criterion to evaluate this kinematic performance is the GCI. For a workspace distributed over a region Ω, the GCI is defined as [15]

$$GCI = \frac{\int_\Omega 1/\kappa(\mathbf{J})dw}{\int_\Omega dw} \tag{20}$$

with the condition number $\kappa(\mathbf{J})$ is defined as

$$\kappa(\mathbf{J}) = \|\mathbf{J}^{-1}\|\|\mathbf{J}\| \tag{21}$$

where the Euclidean norm $\|\cdot\|$ of a matrix $\mathbf{A}$ is

$$\|\mathbf{A}\| = \sqrt{tr(\mathbf{A}^T\mathbf{W}\mathbf{A})} \tag{22}$$

with $\mathbf{W} = \frac{1}{3}\mathbf{I}$ for the purpose of normalization. Here $\mathbf{I}$ is the 3×3 identity matrix. In practice, the GCI of an SPM is calculated through a discretized approach, i.e.

$$GCI = \frac{1}{W}\sum_{i=1}^{n}\frac{1}{\kappa_i}\Delta w_i \tag{23}$$

where n is the total number of discretizing points and W is the volume of workspace.

In order to get an accurate value of GCI, one has to visit as many points (orientations) within a workspace as possible. In addition, a system of highly nonlinear equations has to be solved for each point to find joint variables. For these reasons, the calculation of GCI is computational intensive and time-consuming. Hence it is not practical, at least not efficient, to find optimal GCI by any exhausted searching approach. The author hence resorts to the numerical optimization technique for an optimal solution, with a wish to avoid searching the design space exhaustedly. In doing so, the evaluation criterion, GCI, is modified so that the new criterion is suitable for numerical optimization, as outlined presently.

Referring to Eq. (23), the volume of the orientational workspace can be partitioned equivolumetrically, i.e., $\Delta w_i \equiv \Delta w$, as reported in [24]. With such a measure, Eq. (23) becomes

$$GCI = \frac{1}{n}\sum_{i=1}^{n}\frac{1}{\kappa_i} \tag{24}$$

The conditioning index obtained through Eq. (24) is an arithmetic mean, which can be replaced with a quadratic mean for a better indication of the dexterity. Moreover, a quadratic function can lead to a least squares problem, which is readily solved. A new conditioning index is therefore defined as

$$C_a = \frac{1}{n}\sum_{i=1}^{n}\frac{1}{\kappa_i^2} \tag{25}$$

Now that $\kappa_i \geqslant 1,\ C_a$ is a positive number with an upper bound of 1, the same as the GCI. In view of this, C_a can be regarded as an approximate of GCI.

The condition number κ of Eq. (25), by definition, is a function of geometrical parameters as well as configuration variables. The condition number can be expressed as

$$\kappa = \kappa(\alpha_1, \alpha_2, \beta, \gamma, \theta_1, \theta_2, \theta_3, \psi_1, \psi_2, \psi_3) = \kappa(\mathbf{x}; \boldsymbol{\theta}; \boldsymbol{\psi}) \tag{26}$$

where the set of geometrical parameters $\mathbf{x} = [\alpha_1, \alpha_2, \beta, \gamma]^T$, the configuration variables $\boldsymbol{\theta} = [\theta_1, \theta_2, \theta_3]^T$ and $\boldsymbol{\psi} = [\psi_1, \psi_2, \psi_3]^T$. In the closed-loop kinematic chain of SPM, $\boldsymbol{\theta}$ is considered as a function of $\boldsymbol{\psi}$, which is implicitly defined by Eq. (8). For any orientation $\boldsymbol{\psi}_i = [\psi_1, \psi_2, \psi_3]_i^T$, the condition number κ_i can be expressed as

$$\kappa_i = \kappa_i(\mathbf{x}) = \kappa(\mathbf{x}; \boldsymbol{\theta}(\boldsymbol{\psi}); \boldsymbol{\psi})|_{\boldsymbol{\psi}=\boldsymbol{\psi}_i} \tag{27}$$

5.2. Optimization

Letting $\mathbf{q} = \mathbf{q}(\mathbf{x}) = \left[\frac{1}{\kappa_1}, \frac{1}{\kappa_2}, \ldots, \frac{1}{\kappa_n}\right]^T$, Eq. (25) is rewritten as

$$C_a = \frac{1}{n}\mathbf{q}^T\mathbf{q} \tag{28}$$

which is the objective function for the numerical optimization problem. To be able to find a reasonable optimal solution, certain constraints have to be included.

Two constraints in connection with closed-loop mechanisms are considered. The first constraint is the multiple solutions of the inverse kinematics. In the case of SPMs, each leg can be regarded as a part of four-bar spherical linkage, which has two branches for a given orientation, as indicated in Fig. 4. The SPM thus has totally eight sets of solutions of joint angles. In the optimization, the joint angle may take any branch, if no constraint is applied. To make sure the manipulator can virtually move continuously, a constraint on the system has to be added to the system to force the legs belonging to a certain branch. From the point of view of kinematics, each leg shall keep the same branch as the initial position, unless it passes a singular point.

A careful observation on the mechanism finds that each leg stays with one branch until vectors $\mathbf{u}_i$, $\mathbf{w}_i$ and $\mathbf{v}_i$ are coplanar. If we constrain the sign of $(\mathbf{u}_i \times \mathbf{w}_i) \cdot \mathbf{v}_i$, the joint variable will be confined to one branch only.

The second constraint comes from the closure of the kinematic chain. The kinematic chain has to be closed for SPMs at any orientation of the mobile platform in order to make the mechanism physically feasible. The closed-loop chain condition can be satisfied through Eq. (8). Based on the above two constraints, the optimum problem is finally formulated as

$$\begin{aligned} \max_{\mathbf{x}} \quad & \frac{1}{n}\mathbf{q}^T\mathbf{q} \\ \text{s.t.} \quad & \mathbf{w}_i \cdot \mathbf{v}_i - \cos\alpha_2 = 0 \\ & (\mathbf{u}_i \times \mathbf{w}_i) \cdot \mathbf{v}_i \leqslant 0 \end{aligned} \tag{29}$$

which is a nonlinear least squares problem that can be solved by many commercial available optimization codes.

As a matter of fact, the constraints in Eq. (29) also apply to the function f_i of Eq. (18b), thereby the maximum and minimum of f_i can be obtained numerically based on these constraints.

6. Design examples

Three examples are included in this section to demonstrate the application of the proposed optimum design method. While many commercial optimization codes are available, the optimization package with Maple 10 is selected in this work to carry out numerical optimization. A built-in solver under the name '`LSSolve`' is used to solve the nonlinear least squares problems at hand.

6.1. Example I

The first example deals with an SPM with coaxial input shafts, as the case of the active ball joint, i.e., $\gamma = 0$. The prescribed workspace is assumed as a pointing cone of 120° opening with 360° full rotation. The design variables are taken as

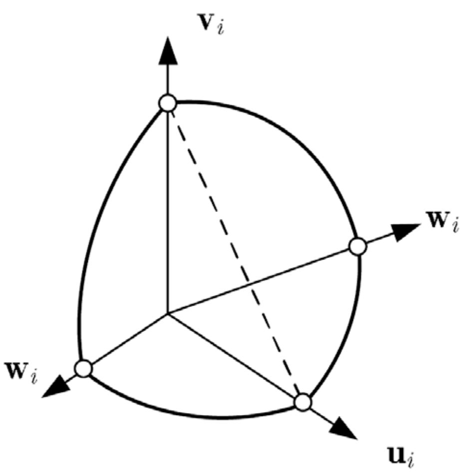

Fig. 4. The two branches of a leg of an SPM.

$\mathbf{x} = [\alpha_1, \alpha_2, \beta]^T$. The total number of points used for optimization is $n = n_1 \times n_2 \times n_3$, where $n_1,\ n_2$ and n_3 are numbers of discretizing points on $\psi_1,\ \psi_2$ and ψ_3, respectively. In the example, totally $4 \times 12 \times 3 = 144$ points are selected. For each discretizing point, the two constraints of Eq. (29) yield six inequalities, in which $\mathbf{u}_i,\ \mathbf{w}_i$ and $\mathbf{v}_i$ are obtained through Eqs. (3), (5) and (6), respectively. Note that $\theta_i,\ i = 1, 2, 3$, are not calculated explicitly, but treated as dependent variables of ψ_i satisfying Eq. (8). All discretizing points thus lead to $144 \times 6 = 864$ inequalities in total, all being the functions of the design variables.

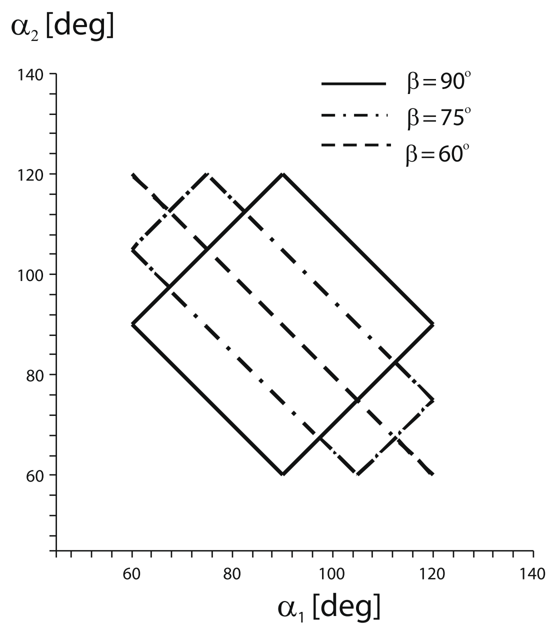

Fig. 5. Design space of an SPM.

Table 1
Optimization of an SPM with coaxial input shafts.

α_1 (°)	α_2 (°)	β (°)	C_a
60.0 (120.0)	90.0	90.0	0.28

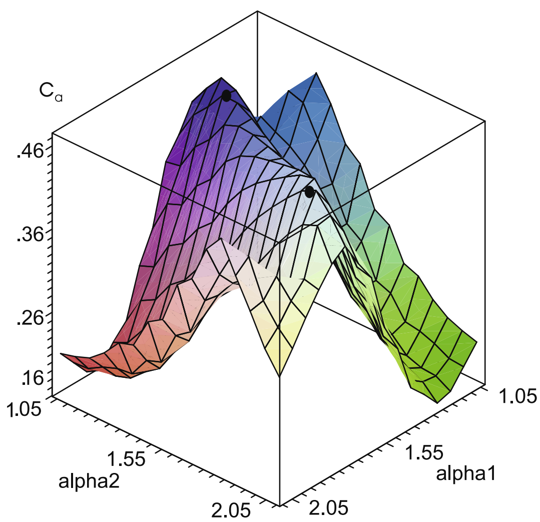

Fig. 6. Distribution of conditioning index with $\beta = 75°$.

The design space is determined first upon the solution of the bounds of f_i. For $\beta = 75^\circ$, the lower and upper bounds of f_i are found to be $f_{min} = -0.707$ and $f_{max} = 0.966$. The design space inequalities are hence $|\alpha_1 - \alpha_2| \leqslant 45^\circ$ and $|\alpha_1 + \alpha_2 - 180^\circ| \leqslant 15^\circ$. By taking different values of β, other inequalities of the design space can be found accordingly. Shown in Fig. 5 are sub-design spaces with β = 90°, 75° and 60°. It is observed that the design space with $\beta = 60^\circ$ degenerates into a

Table 2
Comparison of optimization results with two methods.

	α_1 (°)	α_2 (°)	β (°)	$1/\kappa$
Numerical method	48	90	90	0.72
Graphic method	50	105	75	0.67

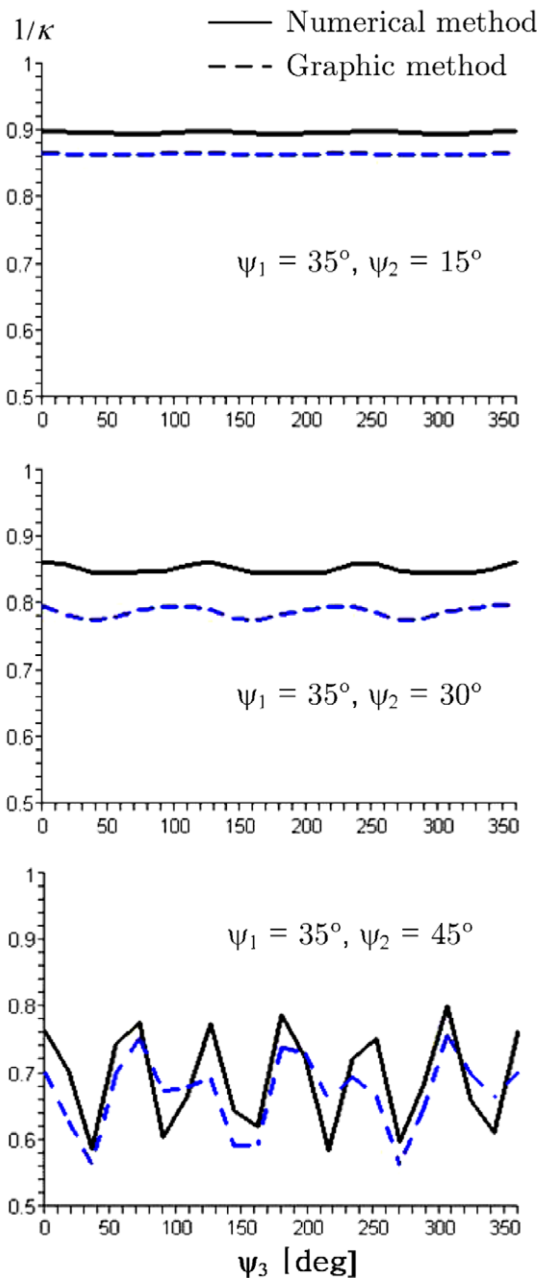

Fig. 7. The variation of conditioning index over a full rotation.

line segment, which gives the limit of β. As a matter of fact, $f_{max} = 1.0$ for $\beta = 60^\circ$, from which the inequality (19b) becomes an equation $\alpha_1 + \alpha_2 = 180^\circ$. The line-shape design space implies that the value of β has to be at least 60° in order to attain orientations in the prescribed workspace. The entire design space for the prescribed workspace can be obtained by enveloping all sub-design spaces with different values of β.

The optimization with Eq. (29) is carried out with feasible initial values, which are taken from the design space determined by the design space inequalities. In this work, the convex of Fig. 5 are used as initial points. With different initial values, two optima which are different in α_1 only, but with an identical value of $C_a = 0.28$, are found. The optima are listed in Table 1, where the second set of optimum is included in parenthesis. Note that two dimensions are supplementary. This implies that they stand for the same design but different configurations.

An optimization may end up with local minima or maxima. In the case of SPM optimization, the optimization process starts with different initial points taken in the design space. Each point yields an optimum; the solution is taken as the one with the maximum objective values. Note that there may exist more than one optimal solutions, as shown in Fig. 6. Two optima, which are dotted in the figure, have identical objective values. Both optima are the optimal solutions, which correspond to two configurations of an SPM.

In most situations, a workspace free of singularity is preferred. To this end, an additional constraint can be included in Eq. (29). For example, to eliminate the singularity which occurs within the workspace, i.e., the type II singularity [25], one more constraint can be included as

$$[\det(\mathbf{A})]^2 \geqslant \Delta \tag{30}$$

where $\mathbf{A} = [\mathbf{a}_1, \mathbf{a}_2, \mathbf{a}_3]^T$ with $\mathbf{a}_i = \mathbf{w}_i \times \mathbf{v}_i$ and Δ is a previously established tolerance. In this example, the author has included this additional constraint in the optimization, the same optimal result being obtained.

It is noted that the optimum obtained by the proposed method is confined by prescribed workspace. As readers may find, the optimum C_a in the example is relatively small for the given workspace. In such a case of small C_a, it may suggest that a review of the design specifications is necessary for a high dexterity.

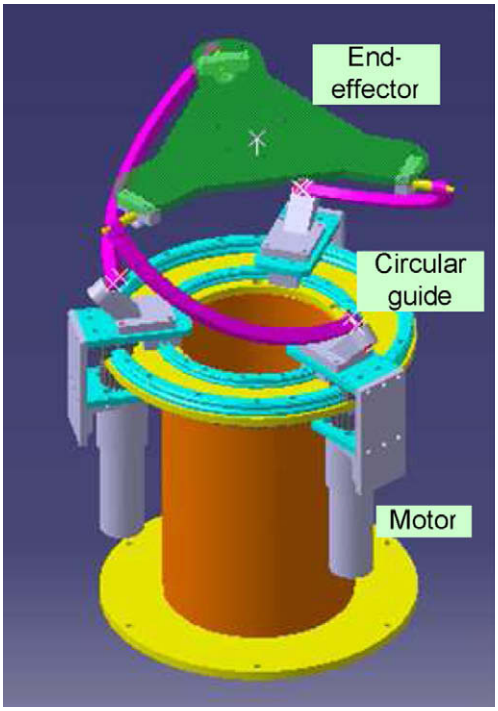

Fig. 8. CAD model of an SPM capable unlimited rolling.

Table 3
Optimization of an SPM with identical base and mobile platforms.

α_1 (°)	α_2 (°)	β (°)	γ (°)	C_a
54.9 (115.4)	115.4 (54.9)	33.3	33.3	0.585

6.2. Example II

In this example, the proposed optimization method is examined with the spherical wrist reported in [11], which has a prescribed workspace of a conic opening of 90° and 360° full rotation. Following the same approach as the first example, the optimal result is obtained as given in Table 2. The optimal result reported in [11], in which a graphic method was employed, is also included in the same table for information. Based on the two optima, the variations of their conditioning indices over a full cycle of rotation are plotted in Fig. 7. It is clearly seen the difference in the variations of conditioning indices with both $\psi_2 = 15^\circ$ and $\psi_2 = 30^\circ$. For the numerical optimization result, the rms value of $1/\kappa$ over the discretizing points is 0.72, comparing with 0.67 for the graphically optimized result, which indicates an improvement in the dexterity.

The optimum results with this example are selected for the active ball joint. The CAD model of the active ball joint is shown in Fig. 8. In the design, sliders move together with motors via pinion and gear-ring transmissions. Two sets of HCR guides from THK are used to enable sliders' high-precision circular motion with small clearance.

6.3. Example III

The above two examples deal with spherical parallel manipulators with coaxial input shafts. The method can also be applied to general spherical parallel manipulators. An extra example is included, which is a spherical parallel manipulator with identical pyramids for the base and mobile platforms. The prescribed workspace is a 90° conic opening with 30° in torsion. The design variables are taken as $\mathbf{x} = [\alpha_1, \alpha_2, \beta, \gamma]^T$. One more constraint $\gamma - \beta = 0$ is added to Eq. (29) for the identical base and mobile platforms. Table 3 presents the optimization results.

Note that there are two sets of optimal parameters with an identical C_a, similar to the case of the active ball joint. Standing for two possible configurations of a SPM, the two solutions provide flexibility of dimension selection in mechanical designs.

7. Discussion and conclusions

The optimum design of spherical parallel manipulators for a prescribed workspace is studied. The design space of a spherical parallel manipulator for the prescribed workspace is found through a system of inequalities. The design space enables a designer to select feasible design parameters for modeling of a spherical parallel manipulator. Moreover, the design space helps also to reduce the searching space in optimization of spherical parallel manipulators. Thus it can be expected to find its applications in classes of optimizations.

A numerical optimization method is introduced to find optimal design parameters in terms of dexterity. An objective function is formulated by modifying the conditioning index so that the optimization problem is converted to a nonlinear least squares problem, which is readily solved with commercially available software. Compared with graphical methods, the numerical method can handle effectively with the design space containing more design variables, the number of which, in the case of this study, is equal to four. The method can also save the intensive searching efforts that are required for the searching techniques. Moreover, the optimization method formulated in the form of a least squares problem is numerically robust and readily solved. Constraints with respect to the closed-loop kinematic chain are derived. The design examples show that the proposed method is able to find the optimal solution.

References

[1] C.M. Gosselin, J.F. Hamel, The Agile Eye: a high-performance three-degree-of-freedom camera-orienting device, in: IEEE International Conference on Robotics and Automation, 1994, pp. 781–786.
[2] T. Li, S. Payandeh, Design of spherical parallel mechanisms for application to laparoscopic surgery, Robotica 20 (2) (2002) 133–138.
[3] E. Cavallo, R.C. Michelini, A robotic equipment for the guidance of a vectored thrustor, in: 35th International Symposium on Robotics (ISR 2004), Paris, 2004.
[4] M. Carricato, V. Parenti-Castelli, A novel fully decoupled two-degrees-of-freedom parallel wrist, The International Journal of Robotics Research 23 (6) (2004) 661–667.
[5] J.-P Merlet, Jacobian, manipulability, condition number, and accuracy of parallel robots, ASME Journal of Mechanical Design 128 (1) (2006) 199–206.
[6] X. Kong, C.M. Gosselin, Type synthesis of three-degree-of-freedom spherical parallel manipulators, The International Journal of Robotics Research 23 (3) (2004) 237–245.
[7] X.J. Liu, Z.L. Jin, F. Gao, Optimum design of 3-DOF spherical parallel manipulators with respect to the conditioning and stiffness indices, Mechanism and Machine Theory 35 (9) (2000) 1257–1267.
[8] I.A. Bonev, C.M. Gosselin, Analytical determination of the workspace of symmetrical spherical parallel mechanisms, IEEE Transactions on Robotics 22 (5) (2006) 1011–1017.
[9] C.M. Gosselin, J. Angeles, The optimum kinematic design of a spherical three-degree-of-freedom parallel manipulator, ASME Journal of Mechanisms, Transmissions, and Automation in Design 111 (1989) 202–207.
[10] S. Leguay-Durand, C. Reboulet, Optimal design of a redundant spherical parallel manipulator, Robotica 15 (4) (1997) 399–405.
[11] H. Asada, J. Granito, Kinematic and static characterization of wrist joints and their optimal design, in: IEEE International Conference on Robotics and Automation, 1985, pp. 244–250.
[12] R. Kurtz, V. Hayward, Multiple-goal kinematic optimization of a parallel spherical mechanism with actuator redundancy, IEEE Transactions on Robotics and Automation 8 (5) (1992) 644–651.
[13] M. Trabia, J.K. Davidson, Design conditions for the orientation and attitude of a robot tool carried by a 3-R spherical wrist, ASME Journal of Mechanisms, Transmissions, and Automation in Design 111 (1989) 176–187.
[14] J.K. Salisbury, J.J. Craig, Articulated hands, force control and kinematic issues, International Journal of Robotics Research 1 (1) (1982) 4–17.

[15] C.M. Gosselin, J. Angeles, A global performance index for the kinematic optimization of robotic manipulators, ASME Journal of Mechanical Design 113 (3) (1991) 220–226.
[16] K.C. Gupta, B. Roth, Design considerations for manipulator workspace, ASME Journal of Mechanical Design 104 (4) (1983) 704–711.
[17] J.K. Davidson, K.H. Hunt, Rigid body location and robot workspace: some alternative manipulator forms, ASME Journal of Mechanisms, Transmissions, and Automation in Design 109 (2) (1987) 224–232.
[18] J.J. Cervantes-Sanchez, J.C. Hernandez-Rodriguez, J. Angeles, On the kinematic design of the 5R planar, symmetric manipulator, Mechanism and Machine Theory 36 (11) (2001) 1301–1313.
[19] X.J. Liu, J. Wang, A new methodology for optimal kinematic design of parallel mechanisms, Mechanism and Machine Theory 42 (9) (2007) 1210–1224.
[20] P. Zsombor-Murray, Kinematic mapping and kinematics of some parallel manipulators, in: Proceedings of the Second International Workshop on Fundamental Issues and Future Research Directions for Parallel Mechanisms and Manipulators, September 21–22, Montpellier, France, 2008.
[21] J. Kim, J.C. Hwang, et al, Eclipse II: a new parallel mechanism enabling continuous 360-degree spinning plus three-axis translational motions, IEEE Transactions on Robotics and Automation 18 (3) (2002) 367–373.
[22] F. Janabi-Sharifi, B. Shchokin, A rotary parallel manipulator: modeling and workspace analysis, in: IEEE International Conference on Robotics and Automation, 2004, pp. 3671–3677.
[23] http://www.en.wikipedia.org/wiki/Rotation_matrix.
[24] G.L. Yang, I.M. Chen, Equivolumetric partition of solid spheres with applications to orientation workspace analysis of robot manipulators, IEEE Transactions on Robotics 22 (5) (2006) 869–879.
[25] C.M. Gosselin, J. Angeles, Singularity analysis of closed-loop kinematic chains, IEEE Transactions of Robotics and Automation 6 (3) (1990) 281–290.